Evidence of the water-cage effect on the photolysis of NO3- and [FeOH]2+. Implications of this effect and of H2O2 surface accumulation on photochemistry at the air-water interface of atmospheric droplets.

Evidence of the water-cage effect on the photolysis of NO_3^- and $FeOH^{2+}$, and its implications for the photochemistry at the air-water interface of atmospheric droplets

P. Nissenson,[1] D. Dabdub,[1,*] R. Das,[2,3] V. Maurino,[2] C. Minero[2] and D. Vione [2,*]

[1] Department of Mechanical and Aerospace Engineering, University of California, Irvine, CA, USA.

[2] Dipartimento di Chimica Analitica, Università degli Studi di Torino, Via P. Giuria 5, 10125 Torino, Italy. *http://www.chimicadellambiente.unito.it*

[3] Department of Chemical Engineering, Haldia Institute of Technology, ICARE complex, Haldia 721657, India.

* Address correspondence to either author: D. Dabdub (ddabdub@uci.edu)
or D. Vione (davide.vione@unito.it) *http://chimica.campusnet.unito.it/cgi-bin/docenti.pl/Show?_id=dvione*

Abstract

Experiments are conducted to determine the effect of a cage of water molecules on the photolysis quantum yields of nitrate, $FeOH^{2+}$, and H_2O_2. Results suggest that the quantum yields of nitrate and $FeOH^{2+}$ are decreased by the recombination of photo-fragments ($^{\bullet}OH$ + $^{\bullet}NO_2$ and Fe^{2+} + $^{\bullet}OH$, respectively) before they leave the surrounding cage of water molecules. However, no evidence is found for an enhanced quantum yield for H_2O_2. Therefore, the photolysis of nitrate and $FeOH^{2+}$ could be enhanced if the cage of the solvent molecules is incomplete, as is the case at the air-water interface of atmospheric droplets. The photolysis rate constant distribution within nitrate, $FeOH^{2+}$, and H_2O_2 aerosols is calculated by combining the expected quantum yield data in the bulk and at the interface with Mie theory calculations of light intensity. The photolysis rate constant of nitrate and $FeOH^{2+}$ would be significantly higher at the surface than in the bulk if quantum yields are enhanced at the surface. In the case of H_2O_2, the photolysis rate constant would be enhanced by surface accumulation. The results concerning the expected rates of photolysis of these photoactive species are applied to the assessment of the reaction between benzene and $^{\bullet}OH$ in the presence of $^{\bullet}OH$ scavengers in an atmospherically relevant scenario. For a droplet of 1 μm radius, a large fraction of the total $^{\bullet}OH$-benzene reaction (15% for H_2O_2, 20% for nitrate, and 35% for $FeOH^{2+}$) would occur in the surface layer, which accounts for just 0.15% of the droplet volume.

Keywords: solvent-cage; photochemistry; quantum yield; semi-volatile organic compounds; Mie theory

1. Introduction

The photo-chemical reactions that take place in water droplets may play an important role in atmospheric chemistry, including the formation and transformation of major organic components and pollutants (Jacob, 2000; Vione et al., 2006; Amato et al., 2007; Vione et al., 2009a). Two major issues arise in studying these reactions. The first issue is that the actinic flux inside small water droplets can be considerably higher than in the surrounding gas phase because of refraction and diffraction phenomena (Madronich, 1987). Estimates for the enhancement factor vary from 1.5 to 2 (Madronich, 1987; Ruggaber et al., 1997; Mayer and Madronich, 2004; Nissenson et al., 2006).

The second issue is that some reactions are faster at the air-water interface than in the solution bulk (Hu et al., 1995; Knipping et al., 2000). An interface enhancement also has been observed in the case of the photo-chemical reactions (Furlan, 1999; Winter and Benjamin, 2004), and a recent study into the photolysis of $Mo(CO)_6$ in 1-decene droplets has provided evidence that a large part of the effect is accounted for by the incomplete cage of the solvent molecules at the interface (Nissenson et al., 2006). In the solution bulk, the fragments that are generated by photolysis are initially surrounded by the cage of the solvent molecules, and their diffusion out of the cage is in competition with regeneration of the photoactive compound through recombination. The effect of the recombination reactions is that of decreasing the photolysis quantum yields in the solution bulk. At the interface, the solvent-cage is incomplete and the recombination reactions are inhibited as a consequence. Therefore, the photolysis quantum yields could be higher at the interface than in the bulk. For instance, the incomplete cage of water molecules enhances the photochemistry of nitrate in deliquesced mixtures of NaCl and $NaNO_3$ (Wingen et al., 2008).

The quantification of the solvent-cage effect in aqueous solution presents a number of experimental difficulties, which could explain why limited data are available on the topic. However, evidence that the recombination processes decrease the photolysis quantum yields has been obtained in the case of nitrate (Warneck and Wurzinger, 1988; Bouillon and Miller, 2005; Chiron et al., 2009; Das et al., 2009; Vione et al,, 2009b) and $FeCl^{2+}$ (Khanra et al., 2008).

To our knowledge, no assessment presently is available of the possible impact of the described interface phenomena on the photo-chemical reactions that take place in water droplets in the atmosphere. This is the purpose of the present paper, in which the effect of the solvent-cage on the photolysis quantum yields of nitrate, $FeOH^{2+}$ and H_2O_2 is studied upon

addition of 2-propanol as $^{\bullet}OH$ scavenger. Quantum yields with and without the effect of the cage of water molecules on recombination processes is determined through experiments and, together with Mie theory calculations for light intensity, are used to calculate the expected photolysis rate constants of nitrate, $FeOH^{2+}$ and H_2O_2 at atmospherically relevant concentrations inside water droplets illuminated by actinic radiation. The results concerning the rates of photolysis of these photoactive species are applied to the assessment of the reaction between benzene and $^{\bullet}OH$, in the presence of $^{\bullet}OH$ scavengers in an atmospherically relevant scenario.

2. Experimental

The adopted reagents are reported as Supplementary Material. Samples to be irradiated (5 mL total volume) are placed in Pyrex glass cells (4.0 cm diameter, 2.3 cm height) and magnetically stirred during irradiation. Irradiation is carried out under UV lamps. One of the lamps has emission maximum at 313 nm (Philips TL 01) with 5.6±0.4 W m^{-2} irradiance, measured with a CO.FO.ME.GRA. (Milan, Italy) power meter, which corresponds to $(3.7\pm0.3)\times10^{-6}$ einstein L^{-1} s^{-1} in solution, actinometrically determined using the ferrioxalate method (Kuhn et al., 2004). The other lamp (Philips TLK05) has an emission maximum at 365 nm with 5.5±0.3 W m^{-2} irradiance, corresponding to $(4.2\pm0.2)\times10^{-6}$ einstein L^{-1} s^{-1} in solution. The absorption spectra of nitrate, H_2O_2, and Fe(III), the latter taken with a Varian Cary 100 Scan UV-Vis spectrophotometer at pH 2.5, are reported in Figure 1. The temperature of the irradiated solutions is approximately 30°C.

The determination of acetone formation from 2-propanol is carried out by pre-column derivatization with 2,4-dinitrophenylhydrazine (10 min contact time; Warneck and Wurzinger, 1988), followed by analysis of the resulting hydrazone with High Performance Liquid Chromatography coupled with Diode Array Detection (HPLC-DAD). Nitrite is determined by derivatization with 2,4-dinitrophenylhydrazine also (10 min contact time; Kieber and Seaton, 1996), followed by HPLC-DAD determination of the azide formed. Further details are reported as Supplementary Material.

Dark runs are conducted by placing cells wrapped in aluminum foil under the same lamps used in the irradiation experiments to achieve similar temperature and stirring conditions among dark and illuminated systems. Negligible formation of acetone from 2-propanol is observed in these dark runs and similar results are obtained by irradiation of 2-propanol alone, without the photoactive compounds.

Fe^{2+} is determined with a Varian Cary 100 Scan UV-Vis spectrophotometer, as complex with 1,10-phenanthroline (absorption maximum at 510 nm) (Kuhn et al., 2004).

The time evolution data of nitrite and acetone are fitted with equations of the form $[I]_t = k^f_I [S]_0 (k^d_I - k^d_S)^{-1} [exp(-k^d_S\, t) - exp(-k^d_I\, t)]$, where $[I]_t$ is the concentration of the intermediate (nitrite or acetone) at the time t, $[S]_0$ the initial concentration of the substrate (nitrate or 2-propanol), k^f_I and k^d_I the pseudo-first order rate constants for the formation and degradation of the intermediate, and k^d_S the pseudo-first order rate constant for the degradation of the substrate. The initial formation rate of the intermediate is given by $R_I = k^f_I [S]_0$. The error bounds associated to the rate data represent $\mu \pm \sigma$, derived from the fit of the theoretical curves to the experimental data (intra-series variability). The reproducibility of repeated runs (inter-series variability) is approximately 10-15%.

3. Results and Discussion

3.1. Water-cage effect on the photolysis quantum yields

Figure 2 reports the initial formation rates of nitrite and acetone ($(CH_3)_2CO$) upon UVB irradiation of 0.01 M $NaNO_3$, as a function of the concentration of 2-propanol ($(CH_3)_2CHOH$). Figure 2 shows that the increase of the formation rates between low or no propanol and high propanol is approximately 2 and 3.8 times for nitrite and acetone, respectively. The following processes account for the formation of nitrite and acetone in the system (Warneck and Wurzinger, 1988; Mark et al., 1996; Mack and Bolton, 1999):

$$NO_3^- + h\nu + H^+ \rightleftarrows [{}^\bullet OH + {}^\bullet NO_2]_{cage} \rightarrow {}^\bullet OH + {}^\bullet NO_2 \quad (1)$$

$$NO_3^- + h\nu \rightarrow NO_2^- + O \quad (2)$$

$$2\ {}^\bullet NO_2 \rightleftarrows N_2O_4 \quad (3)$$

$$N_2O_4 + H_2O \rightarrow NO_3^- + NO_2^- + 2\ H^+ \quad (4)$$

$$O + NO_3^- \rightarrow O_2 + NO_2^- \quad (5)$$

$$(CH_3)_2CHOH + {}^\bullet OH \rightarrow (CH_3)_2C{}^\bullet OH + H_2O \text{ or other intermediates} \quad (6)$$

$$(CH_3)_2C{}^\bullet OH + O_2 \rightarrow (CH_3)_2CO + HO_2{}^\bullet \quad (7)$$

$$(CH_3)_2CHOH + O \rightarrow (CH_3)_2C{}^\bullet OH + {}^\bullet OH \quad \text{or} \quad (CH_3)_2CO + H_2O \quad (8)$$

After photo-induced formation, the radicals ${}^\bullet OH$ and ${}^\bullet NO_2$ may undergo geminate recombination when they are still inside the cage of water molecules, reforming nitrate. This would decrease the quantum yield of nitrate photolysis (Mark et al., 1996; Warneck and Wurzinger, 1988). At elevated [2-propanol], the reaction between the alcohol and ${}^\bullet OH$ inside the water cage could reduce the in-cage recombination between ${}^\bullet OH$ and ${}^\bullet NO_2$, enhancing as a consequence the formation of both acetone and nitrite. Note that the recombination of ${}^\bullet OH$ and ${}^\bullet NO_2$ outside the solvent-cage at elevated [2-propanol] is unlikely because of the

scavenging of $^{\bullet}OH$ by the alcohol. Moreover, detailed calculations for $^{\bullet}OH + {}^{\bullet}NO_2$ by Minero et al. (2007) showed that the recombination of $^{\bullet}OH$ and $^{\bullet}NO_2$ in the solution bulk would be negligible also in the absence of 2-propanol.

Warneck and Wurzinger (1988) showed that the kinetics of acetone formation is a better measure of the quantum yield of $^{\bullet}OH$ photoproduction, $\Phi(^{\bullet}OH)$, than that of nitrite. It has been shown that $\Phi(^{\bullet}OH) = 1.15\ \Phi(\text{Acetone})$ (Warneck and Wurzinger, 1988), where $\Phi(\text{Acetone}) = R_{\text{Acetone}}\ (P_{a,NO3-})^{-1}$, and $P_{a,NO3-}$ is the photon flux absorbed by nitrate. By application of the Lambert-Beer law one gets $P_{a,NO3-} = 6\times10^{-8}$ einstein $L^{-1}\ s^{-1}$ for 0.01 M NO_3^-. This study finds $\Phi(^{\bullet}OH) \approx 0.01$ at low [2-propanol], and $\Phi(^{\bullet}OH) = 0.034$ at elevated [2-propanol]. Note that Mark et al. (1996) irradiated nitrate solutions at 254 nm in the presence of 2-propanol, varying the concentration of the alcohol over many orders of magnitude. They also find a considerable change in the formation rate of nitrite, which they attribute to a changing solvent-cage effect. A comparison between the present results and those obtained in previous studies (Zepp et al., 1987; Warneck and Wurzinger, 1988; Zellner et al., 1990; Mark et al., 1996; Goldstein and Rabani, 2007) is reported in the Supplementary Material.

Figure 3 reports R_{Acetone} vs. [2-propanol] upon irradiation of 0.1 mM $Fe(ClO_4)_3$ at pH 2.5, where the most important photoactive species of Fe(III) is $FeOH^{2+}$ (Mazellier et al., 1997).

$$FeOH^{2+} + h\nu \rightleftarrows [Fe^{2+} + {}^{\bullet}OH]_{cage} \rightarrow Fe^{2+} + {}^{\bullet}OH \qquad (9)$$

From the reported stability constants of the Fe^{3+}/OH^- complexes (Martell et al., 1997) one finds $[FeOH^{2+}] > [Fe^{3+}] >> [Fe(OH)_2^+]$ at pH 2.5. In addition, $FeOH^{2+}$ produces $^{\bullet}OH$ with much higher quantum yield than Fe^{3+} (Benkelberg and Warneck, 1995), thus the reported results would reflect the photochemistry of $FeOH^{2+}$.

Considering that Fe(III) cannot scavenge $^{\bullet}OH$ and that Fe^{2+} is produced in too low concentration to compete with 2-propanol (also see Supplementary Material), the alcohol would be the only species to react with $^{\bullet}OH$ significantly. Under such conditions one would expect the formation rate of acetone to reach a plateau quickly in the absence of the solvent-cage effect. The increase of the initial formation rate of acetone with increasing [2-propanol] provides evidence of a reaction between the alcohol and $^{\bullet}OH$ inside the cage of the water molecules. By reacting with cage $^{\bullet}OH$, 2-propanol would inhibit the cage recombination between Fe^{2+} and $^{\bullet}OH$. The formation rate of acetone would be enhanced as a consequence.

Interestingly, the formation rate of acetone is considerably higher under UVB irradiation (emission maximum at 313 nm) than under UVA (emission maximum at 365 nm). The formation of acetone from 2-propanol would be a direct measurement of the $^{\bullet}OH$ yield from $FeOH^{2+}$, which would also be the main absorbing species in the wavelength ranges adopted

for irradiation (Benkelberg and Warneck, 1995). From $\Phi(^{\bullet}OH) = R_{Acetone}\ (P_{a,Fe(III)})^{-1}$ it is possible to derive $\Phi(^{\bullet}OH) = 0.14$ (low [2-propanol]) and $\Phi(^{\bullet}OH) \approx 1$ (high propanol) under UVB (emission maximum at 313 nm), and $\Phi(^{\bullet}OH) = 0.04$ (low propanol) and $\Phi(^{\bullet}OH) = 0.18$ (high propanol) under UVA (emission maximum at 365 nm). Note that from the Lambert-Beer law, $P_{a,Fe(III)} = 6\times10^{-8}$ einstein L^{-1} s^{-1} is obtained under UVB irradiation and $P_{a,Fe(III)} = 3\times10^{-8}$ einstein L^{-1} s^{-1} under UVA irradiation.

Figure 4 reports $R_{Acetone}$ vs. [2-propanol] upon UVB irradiation of 0.01 M H_2O_2. Based on $R_{Acetone}$ at high 2-propanol, one finds that $\Phi(^{\bullet}OH)$ from H_2O_2 photolysis is approximately 1. This value is consistent with Zellner et al. (1990) who found $\Phi(^{\bullet}OH) \approx 0.96$-$0.98$ over 308-351 nm. $R_{Acetone}$ upon irradiation of the H_2O_2 solution increases with [2-propanol]. Note that H_2O_2 is able to scavenge as well as produce $^{\bullet}OH$ (reactions 10,11; Finlayson-Pitts and Pitts, 2000).

$$H_2O_2 + h\nu \rightleftarrows [2\ ^{\bullet}OH]_{cage} \rightarrow 2\ ^{\bullet}OH \qquad (10)$$

$$H_2O_2 + {}^{\bullet}OH \rightarrow HO_2^{\bullet} + H_2O \qquad (11)$$

The trend of $R_{Acetone}$ vs. [2-propanol] would be affected by the competition for $^{\bullet}OH$ between H_2O_2 and 2-propanol (the second-order rate constants with $^{\bullet}OH$ are $k_{11} = 2.7\times10^{7}$ M^{-1} s^{-1} and $k_6 = 1.9\times10^{9}$ M^{-1} s^{-1} respectively; Buxton et al., 1988). At low [2-propanol], $^{\bullet}OH$ is scavenged primarily by H_2O_2. As [2-propanol] increases, the alcohol becomes the main $^{\bullet}OH$ scavenger and the initial formation rate of acetone increases. The competition for $^{\bullet}OH$ is accounted for in eq. (12):

$$\left(\frac{d[\text{Acetone}]}{dt}\right)_{t\rightarrow 0} = \frac{R_{^{\bullet}OH}\cdot k_6\cdot[2-\text{Propanol}]}{k_6\cdot[2-\text{Propanol}] + k_{11}\cdot[H_2O_2]} \qquad (12)$$

Figure 4 demonstrates that eq. (12) reproduces the experimental data well. Therefore, the trend of $R_{Acetone}$ as a function of [2-propanol] may be explained by assuming H_2O_2 and 2-propanol compete for $^{\bullet}OH$, without the need to assume a change of $\Phi(^{\bullet}OH)$ from H_2O_2 photolysis.

The possibility that other $^{\bullet}OH$ scavengers could explain the trend of $R_{Acetone}$ vs. [2-propanol] in the cases of nitrate and Fe(III), in analogy with H_2O_2, is discussed and excluded in the Supplementary Material.

3.2. Radiation absorption and $^{\bullet}$OH generation inside small, spherical water droplets.

Photolysis rate constants are functions of absorber quantum yield, absorber molar absorption coefficient (ε), and the light spectrum. These parameters, in turn, may be functions of wavelength and/or location (for example, bulk versus surface layer). Objects with curved surfaces, such as spherical water droplets, may refract light and create peaks and troughs of light intensity within the object (Bohren and Huffman, 1983; Barber and Hill, 1990). In order to calculate the rate of photolysis within small, spherical droplets, it is necessary to calculate the intensity distribution within the droplets. In the atmosphere, many droplets are similar in size to the wavelength of the incident light and the wave picture of light must be used to calculate the internal intensity distribution (Bohren and Huffman, 1983; Barber and Hill, 1990). This approach, known as Mie theory, has been used in numerous studies to show that the internal intensity distribution is non-uniform and may be enhanced by several orders of magnitude in certain locations due to morphology-dependent resonances, or MDRs (Bohren and Huffman, 1983; Chylek et al., 1985; Benincasa et al., 1987; Barber and Hill, 1990; Ray and Bhanti, 1997; Ruggaber et al., 1997; Mayer and Madronich, 2004; Nissenson et al., 2006).

The numerical model used to calculate the internal intensity distribution is described in Nissenson et al. (2006). Briefly, the light spectrum is discretized into many individual polarized plane-waves which are incident upon an isotropic and homogenous (with respect to angle) spherical water droplet containing absorbers. Careful attention is given to the discretization size so that all MDRs are accounted for. The intensity at a given point within the droplet relative to the incident intensity is,

$$I^{\mathrm{drop,rel}}(\lambda, m, r/a, \theta, \phi) = \frac{mE(m, r/a, \theta, \phi)E^{*}(m, r/a, \theta, \phi)}{E_0^2} \qquad (13)$$

where r , θ, and ϕ are the spherical coordinates, λ is the wavelength, m is the index of refraction, a is the droplet radius, E is the electric field, E^{*} is the complex conjugate of the electric field, and E_0^2 is the incident intensity. The electric field is expressed as an infinite series of vector spherical harmonics and sufficient terms are summed over until convergence is reached.

Droplets in the atmosphere are illuminated non-uniformly over direction. Therefore, a useful quantity is the angle-averaged relative intensity distribution as a function of normalized radius since it is independent of the direction of illumination,

$$I_{\text{ang}}^{\text{drop,rel}}(\lambda, m, r/a) = \frac{\frac{1}{4\pi}\int_0^{2\pi}\int_0^{\pi} mE \bullet E^{*} \sin\theta d\theta d\phi}{E_0^2}, \qquad (14)$$

where the subscript *ang* refers to the angle-averaged relative intensity. At each radial shell, $I_{\text{ang}}^{\text{drop,rel}}(\lambda, m, r/a)$ is calculated for every wavelength. Averaging over all wavelengths yields the angle- and wavelength-averaged intensity distribution as a function of normalized radius,

$$I_{\text{ang},\lambda}^{\text{drop,rel}}(r/a) = \frac{1}{N}\sum_{\lambda} I_{\text{ang}}^{\text{drop,rel}}(m, \lambda, r/a) W(\lambda), \qquad (15)$$

where N is the number of discretizations of the wavelength range and $W(\lambda)$ is a weighting factor that accounts for the actinic flux being a function of wavelength.

The photolysis rate constant of a photoactive species S, $J_{\text{P}}^{\text{S}}(r/a, \theta, \phi)$, is a function of the intensity distribution and therefore is non-uniform throughout the droplet. The angle-averaged photolysis rate constant, $J_{\text{P}}^{\text{S}}(r/a)$, is calculated using $I_{\text{ang}}^{\text{drop,rel}}(m, \lambda, r/a)$ in a manner similar to Ray and Bhanti (1997),

$$J_{\text{P}}^{\text{S}}(r/a) = \sum_{\lambda} G(\lambda)\Phi(\lambda, r/a)\sigma(\lambda) I_{\text{ang}}^{\text{drop,rel}}(m, \lambda, r/a)\Delta(\lambda), \qquad (16)$$

where $G(\lambda)$ is the spectral flux (in units of photons cm^{-2} s^{-1} nm^{-1}). $G(\lambda)$ is multiplied by $I_{\text{ang}}^{\text{drop,rel}}(m, \lambda, r/a)$, which is a measure of the actinic flux enhancement at a particular wavelength.

The index of refraction of the droplet is a function of wavelength and radius, and contains a real and imaginary part. Since the solutes are present in very low concentrations (10^{-4} M or less), the real part of the index of refraction (m_{r}) of the solvent is assumed to be that of water and is calculated using the formula of Quan and Fry (1995). The imaginary part of the index of refraction of the droplet (m_{i}) determines the absorbance of the solution and is calculated in the same manner as Ray and Bhanti (1997),

$$m_{\text{i}}(\lambda, r/a) = m_{\text{i,0}}(\lambda) + \frac{\bar{n}(r)\Phi(\lambda, r/a)\sigma(\lambda)\lambda}{4\pi} N_{\text{a}}, \qquad (17)$$

where $m_{\text{i,0}}(\lambda)$ is the imaginary index of refraction of pure water (taken from Hale and Querry, 1973), $\bar{n}(r)$ is the concentration of the absorber, $\Phi(\lambda, r)$ is the quantum yield of the absorber, $\sigma(\lambda)$ is the absorption cross section of the absorber, and N_{a} is Avogadro's number.

Two different actinic flux spectra are used to calculate the light intensity distribution inside a water droplet. The first spectrum is from Frank and Klöpffer (1988), which is the actinic flux measured over Central Europe (52^{o} N) during June 15^{th} averaged from 8AM to 4PM. The second spectrum is from Finlayson-Pitts and Pitts (2000), which is the theoretical actinic flux value for a solar zenith angle of 30^{o} and an average surface albedo that varies from 0.05 in the 290–400 nm range to 0.15 in the 660–700 nm range. The spectrum in Finlayson-Pitts and Pitts (2000) also is used in Nissenson et al. (2006).

The described methodology allows for the assessment of the rates of photolysis of nitrate, Fe(III), and hydrogen peroxide in atmospheric water droplets. In the case of nitrate, a concentration of 10^{-4} M is adopted which is typical of continental clouds (Warneck, 1999). While initial calculations on the nitrate ion at infinite dilution (Salvador et al., 2003) suggest it has a propensity for the air-liquid interface, more recent studies at finite concentration (Dang et al., 2006) indicate that the ion tends to remain below the surface. Molecular dynamics simulations (Thomas et al., 2007) of nitrate ions in a 1 M solution suggest that nitrate is less solvated close to the interface compared to the bulk. For example, on average there are about 8 water oxygen atoms within 4 Å of the nitrate N in the bulk, but only 6 water oxygen atoms in the case of nitrate near the interface (defined in that study as being within 8 Å of the surface). However, this still may be sufficiently close to the interface that a full solvent shell is not active and enhancement of surface photochemistry could occur.

Due to the uncertainty in the degree of surface segregation of nitrate in water droplets, the authors assume the concentration of nitrate is uniform throughout the droplets in the simulations. If this study overestimates the concentration of nitrate at the surface, the fraction of the processes photo-induced by nitrate that occur at the surface would be reduced.

The non-uniformity of photolysis quantum yields is another issue that must be addressed when calculating the photolysis rate constant distribution within droplets. Nissenson et al. (2006) found experimental evidence for a reduction in the solvent-cage effect at the air-liquid interface when $Mo(CO)_6$ in a 1-decene solvent was irradiated in aerosol form and as a bulk-liquid. Winter and Benjamin (2004) conducted molecular dynamics simulations of ICN in water and found photolysis quantum yields are significantly higher near the surface compared to the bulk. Therefore, it is reasonable to assume that the solvent-cage effect is reduced in the surface layer of water. In this work evidence is found that the cage of the water molecules reduces the photolysis quantum yield of nitrate by a factor of 3.4. Based on the experimental data described before, the photolysis quantum yield adopted for nitrate is 0.01 in the bulk and 0.034 at the surface.

As with $FeOH^{2+}$ and H_2O_2, a surface layer of 0.5 nm thickness is adopted for nitrate, which would make up 0.15% of the volume of a spherical droplet with 1 µm radius. An interface

thickness of approximately five atomic lengths is consistent with molecular dynamics simulations (Winter and Benjamin, 2004; Jungwirth and Tobias, 2006).

In the case of $FeOH^{2+}$, it is possible that the surface concentration might be reduced compared to the bulk, although there is no data to support this. However, doubly charged species likely are not completely repelled from the surface, especially in the presence of organic compounds or anions with some affinity for the surface (Sadiki et al., 2003). It is possible that the surface and bulk concentrations of $FeOH^{2+}$ are equal in the presence of organic compounds such as benzene and formate. Based on the above considerations, a constant concentration of 10^{-6} M (Warneck, 1999) is assumed for $FeOH^{2+}$ throughout the droplet. The same caveats for the nitrate droplet calculations apply for the $FeOH^{2+}$ droplet calculations.

The photolysis quantum yield of $FeOH^{2+}$ varies with wavelength and the wavelength trend is known in the bulk (Benkelberg and Warneck, 1995). Table 1 reports the photolysis quantum yields of $FeOH^{2+}$ adopted here in the case of the bulk (based on data from Benkelberg and Warneck, 1995) and the surface layer (reduced or absent solvent-cage effect). The experimental data of the photolysis quantum yield with reduced or no solvent-cage effect are available for 313 and 365 nm. The values at the other wavelengths are derived by assuming that a similar wavelength trend is operational for the photolysis quantum yield of $FeOH^{2+}$, in the absence and in the presence of the solvent-cage effect.

Hydrogen peroxide is present in continental clouds at 10^{-5} M levels (Warneck, 1999) and has some affinity for the air-water interface. Vacha et al. (2004) report that the concentration of H_2O_2 is enhanced by a factor of two at the air-liquid interface compared to the bulk. Accordingly, the adopted concentration values of H_2O_2 are 1×10^{-5} M in the solution bulk, and 2×10^{-5} M at the surface. As stated earlier, no evidence is found in this work of an effect of the solvent-cage on the photolysis of H_2O_2. Therefore, the adopted value for the photolysis quantum yield of H_2O_2 is 0.5 (corresponding to $\Phi(^{\bullet}OH) = 1$; Finlayson-Pitts and Pitts, 2000), both in the bulk and at the surface.

Figure 5 presents calculations for $I_{ang}^{drop,rel}(r/a)$ using the spectrum from Finlayson-Pitts and Pitts (2000) and the resulting $J_P^{NO_3^-}(r/a)$ for nitrate droplets of three different sizes. The values of $I_{ang}^{drop,rel}(r/a)$ and $J_P^{NO_3^-}(r/a)$ vary little throughout most of the bulk. Near the surface (r/a = 1), $I_{ang}^{drop,rel}(r/a)$ decreases causing $J_P^{NO_3^-}(r/a)$ to decrease as well. However, at the surface layer $J_P^{NO_3^-}(r/a)$ increases sharply due to enhanced quantum yields for nitrate in that region. Similar results are observed for $FeOH^{2+}$ aerosols as this species also has enhanced quantum yields at the surface. For H_2O_2 aerosols, the value of $J_P^{H_2O_2}(r/a)$ at the surface is reduced compared to the bulk because the quantum yield of H_2O_2 is assumed constant throughout the aerosol.

3.3. Assessment of the reaction rate between benzene and •OH

Benzene is chosen as a model aromatic substrate that can undergo accumulation at the air-water interface of atmospheric droplets. There are different estimates for the possible extent of the surface concentration of benzene compared to the bulk (Vacha et al., 2006; Vione et al., 2007), and here an accumulation factor of 75 is assumed. Such a value is not uncommon for aromatic compounds in atmospheric waters (Minofar et al., 2007), the bulk concentrations of which often are in the nM range (Harrison et al., 2005). The adopted concentrations of benzene are 10^{-8} M in the bulk and 7.5×10^{-7} M at the interface.

Atmospheric water droplets contain a wide variety of organic compounds that can act as •OH scavengers and, therefore, can compete with the chosen model molecule for •OH. Among the known droplet components, formate prevails as •OH scavenger (Minero et al., 2007) because of its relatively elevated concentration (typical values for cloud water are around 10^{-5} M; Marinoni et al., 2004) and reaction rate constant ($k_{HCOO^-/\bullet OH} = 3.2\times10^9$ M^{-1} s^{-1}; Buxton et al., 1988). Formate could account for about one half of the total scavenging of •OH in typical continental clouds (Minero et al., 2007) and should be present at about equal concentration in the solution bulk and at the interface (Minofar et al., 2007). For simplicity, in this study it is assumed that the •OH scavengers in water droplets are equivalent to 2×10^{-5} M formate and follow formate's distribution within the droplet. The latter assumption is justified by the fact that the most common •OH scavengers in cloud water are short-chain carboxylic and bicarboxylic acids (Marinoni et al., 2004; Minero et al., 2007). Let J_P^S be the photolysis rate constant of the compound S (NO_3^-, $FeOH^{2+}$ or H_2O_2) to yield •OH, [S] the compound's concentration at the droplet surface or in the bulk, [Benzene] and [Scav] the corresponding concentration values of benzene and the •OH scavengers, respectively ([Scav] = 2×10^{-5} M in the whole droplet), and $k_{scav} = 3.2\times10^9$ M^{-1} s^{-1} and $k_B = 7.8\times10^9$ M^{-1} s^{-1} (Buxton et al., 1988) the respective second-order rate constants for reaction with •OH. The reaction rate between benzene and •OH ($Rate_{B/\bullet OH}$), in competition with the •OH scavengers, would be expressed as follows:

$$Rate_{B/\bullet OH} = J_P^S \cdot [S] \cdot \frac{k_B \cdot [Benzene]}{k_B \cdot [Benzene] + k_{scav} \cdot [Scav]} \qquad (18)$$

Among the variables in eq. (18), $J_P(S)$, [S] and [Benzene] can vary depending on the position inside the droplet (bulk or surface layer). The value of $Rate_{B/\bullet OH}$, expressed in mol L^{-1} s^{-1}, is a function of the distance from the droplet center (r/a) due to the spherical symmetry of the system. The distance r/a varies from 0 to 1, where 0 represents the center and 1 represents the surface. For simplicity issues the surface layer thickness is assumed to be 0.5 nm, equal for

all processes (benzene and H_2O_2 accumulation, interface enhancement of the photolysis quantum yields). To obtain the number of moles of benzene transformed per unit time in the whole droplet or in a part of it, one has to integrate over the volume. Let $F(r/a)$ be the ratio between the number of moles of benzene transformed per unit time inside the spherical section of radius r/a and the total number of moles transformed inside the whole droplet (r/a = 1). $F(r/a)$ can be expressed as follows:

$$F(r/a) = \frac{\int_{o}^{r/a} \left[Rate_{B/\bullet OH}(r/a)\right] \cdot [r/a]^2 \, d(r/a)}{\int_{o}^{1} \left[Rate_{B/\bullet OH}(r/a)\right] \cdot [r/a]^2 \, d(r/a)} \qquad (19)$$

$Rate_{B/\bullet OH}$ is given by eq. (18). Numerical integration of eq. (19) is carried out whenever relevant. Figure 6 reports the trends of $Rate_{B/\bullet OH}(r/a)$ and $F(r/a)$ vs. r/a in the case of 10^{-4} M nitrate. The data are reported for different values of the droplet radius, a = 1, 2, and 3 µm. Figure 6a and 6b are based on the sunlight spectrum reported by Finlayson-Pitts and Pitts (2000) and Frank and Klöpffer (1988), respectively. Note that $Rate_{B/\bullet OH}$ differs by about one order of magnitude in the two cases, while the $F(r/a)$ curves are very similar. The distribution of the reaction within the droplet volume, of which $F(r/a)$ is a measurement, varies very little with the intensity of sunlight. Also note that the trend of $F(r/a)$ vs. r/a shows a continuous increase, followed by a sudden jump to reach $F(r/a)$ = 1 very near the droplet surface. That "jump" is the contribution of the surface layer to the reaction.

The corresponding plots for 10^{-6} M $FeOH^{2+}$ and 10^{-5} M H_2O_2 are reported in Figures 7 and 8, respectively. In the case of droplets with 1 µm radius, a considerable fraction of the total reaction occurs in a surface layer accounting for just 0.15% of the droplet volume. This fraction is about 20% for NO_3^-, 35% for $FeOH^{2+}$, and 15% for H_2O_2. The adopted surface accumulation of benzene is the same in all the cases, thus the differences are linked to the water-cage effect on the photolysis quantum yields of nitrate and $FeOH^{2+}$ and to the surface accumulation of H_2O_2. One caveat to the above analysis is that the increase of the surface reaction rate could be reduced somewhat by the transfer of some photo-fragments to the gas phase, caused by the incomplete solvent-cage at the interface.

3.4. Atmospheric implications

The hydroxyl radicals that react with benzene within the surface layer of atmospheric aerosols could come from either mass transfer from the gas-phase or photolysis of nitrate, Fe(III), or H_2O_2. The rate of mass transfer from the gas-phase to the aqueous phase is given by Schwartz (1986),

$$\frac{d[^{\bullet}OH_{(aq)}]}{dt} = k_{mt}\left([^{\bullet}OH_{(g)}] - \frac{[^{\bullet}OH_{(surf)}]}{HRT}\right), \quad (20)$$

where [$^{\bullet}$OH$_{(surf)}$] is the concentration of $^{\bullet}$OH in the surface layer, [$^{\bullet}$OH$_{(g)}$] is the concentration of $^{\bullet}$OH in the gas-phase, H is the Henry's law constant of $^{\bullet}$OH, R is the universal gas constant, and T is temperature. The first order mass transfer coefficient (k_{mt}) is,

$$k_{mt} = \left(\frac{4a}{3\upsilon\alpha} + \frac{a^2}{3D_g}\right)^{-1}, \quad (21)$$

where a is the droplet radius, υ is the mean molecular velocity, α is the mass accommodation coefficient, and D_g is the gas-phase diffusion constant. For an aerosol of radius a = 1 μm surrounded by air at 298 K, $D_g \approx 2.5\times10^{-5}$ m^2 s^{-1} (Liu et al., 2009) and υ is $(3RT/M)^{1/2}$ = 661 m s^{-1}, where M is the molecular weight of $^{\bullet}$OH. Hanson et al. (1992) report a lower limit for the mass accommodation coefficient of $^{\bullet}$OH, $\alpha > 3.5\times10^{-3}$.

In the extreme case where the aqueous phase concentration is zero and the mass accommodation coefficient is at its highest value (α = 1), k_{mt} is 6.5×10^{7} s^{-1}. During the day, the peak value of [$^{\bullet}$OH$_{(g)}$] is ~10^7 molecules cm^{-3} (Finlayson-Pitts and Pitts, 2000). Therefore, the maximum uptake rate of $^{\bullet}$OH into the aerosol is ~6.5×10^{14} molecules cm^{-3} s^{-1}, or ~1.1×10^{-5} M s^{-1}. However, this is the upper limit of $^{\bullet}$OH uptake into the aerosol. If α = 3.5×10^{-3} and the $^{\bullet}$OH concentration is lower (~10^6 molecules cm^{-3}), the rate of $^{\bullet}$OH uptake would be reduced to 2.8×10^{-9} M s^{-1}.

The photolysis rate constant for nitrate at the surface under actinic irradiation is ~3×10^{-6} s^{-1} (see Figure 5). For a typical concentration of nitrate, 10^{-4} M (Warneck, 1999), the rate of $^{\bullet}$OH production via nitrate photolysis is 3×10^{-10} M s^{-1} at the surface. For Fe(III), the photolysis rate constant at the surface is 1.4×10^{-2} s^{-1}. In the surface layer of an aerosol with a typical concentration of 10^{-6} M Fe(III) (Warneck, 1999), the rate of $^{\bullet}$OH production via $FeOH^{2+}$ photolysis is 1.4×10^{-8} M s^{-1}. For H_2O_2, the photolysis rate constant at the surface is 9.3×10^{-8} s^{-1}. Using similar analysis for an aerosol with a typical H_2O_2 concentration of 2×10^{-5} M (Warneck, 1999), the rate of $^{\bullet}$OH production via H_2O_2 photolysis is 1.9×10^{-12} M s^{-1}.

Therefore, the rate of $^{\bullet}$OH production via photolysis in the surface layer for the nitrate/water and Fe(III)/water droplets may be comparable with the mass transfer of $^{\bullet}$OH from the gas-phase under atmospheric conditions. It appears that $^{\bullet}$OH production via photolysis in the surface layer of H_2O_2/water aerosols may be significantly less than the mass transfer of $^{\bullet}$OH from the gas-phase. However, the analysis above assumes that the aqueous

concentration of $^{\bullet}OH$ is zero, which certainly is not the case in the atmosphere. A non-zero concentration of $^{\bullet}OH$ in the aqueous solution would lower the rate of $^{\bullet}OH$ mass transfer from the gas-phase to the aqueous phase.

4. Conclusions

Evidence is found for an effect of the cage of water molecules on the photolysis quantum yields of nitrate and $FeOH^{2+}$. This study finds that the water-cage effect would decrease the quantum yield of nitrate photolysis by a factor of 3.4 and that of $FeOH^{2+}$ by a factor of 4 to 7, depending on the wavelength range (UVA or UVB). An incomplete solvent-cage is present at the air-water interface of disperse droplets, where the rate of the relevant photo-chemical reactions may be increased compared to the bulk.

In the case of H_2O_2, no evidence is found for a solvent-cage effect on the photolysis quantum yield. However, H_2O_2 would undergo surface accumulation (Vacha et al., 2004) that could enhance photochemistry.

An important consideration is that the light intensity available to photolyze the dissolved compounds is influenced by the droplet geometry, and that the light intensity varies within the droplet volume. Mie theory calculations show that the internal light intensity is enhanced relative to the incident light intensity, with the enhancement lower near the surface compared to the interior. However, the rate of photolysis is significantly higher in the surface layer (0.5 nm thickness) than in the rest of the droplet due to higher quantum yields or surface accumulation.

Modeling of the expected formation and reactivity of $^{\bullet}OH$ in water droplets by photolysis of NO_3^-, $FeOH^{2+}$ and H_2O_2 showed that, in a droplet of 1 μm radius, approximately 15-35% of the total photo-induced reaction would occur in the surface layer (0.5 nm thickness), accounting for just 0.15% of the total volume. In the case of NO_3^- and $FeOH^{2+}$ the rate of photolysis is comparable to that of transfer of $^{\bullet}OH$ from the gas phase into the solution, while the rate of H_2O_2 photolysis is lower.

Interestingly, the volume fraction of the surface layer is inversely proportional to the radius a of the droplet (the droplet volume increases with a^3, that of the surface layer with a^2), and the same trend with a is expected for the fraction of the photo-chemical reaction that takes place in the surface layer. Eqs. (20) and (21) suggest that the rate of transfer of $^{\bullet}OH$ from the gas phase to the solution decreases more quickly than this fraction with increasing a. Therefore, the relative importance of interface photochemistry versus phase transfer would increase with increasing droplet radius. However, for very large droplets the interface photo-chemical reactions would play a secondary role compared to photo-chemical reactions in the bulk.

Acknowledgements

DV, VM and CM acknowledge financial support by MIUR-PRIN 2007 (2007L8Y4NB, Area 02, project n°36), PNRA – Progetto Antartide and Università di Torino – Ricerca Locale. The bursary of RD in Torino was supported by MIUR – Progetto India and by Compagnia di San Paolo. PN and DD acknowledge financial support by the United States National Science Foundation (Grant Nos. CHE-0431312 and ATM-0423804).

References

Amato, P., Demeer, F., Melahoui, A., Fontanella, S., Martin-Biesse, A. S., Sancelme, M., Laj, P., Delort, A. M., 2007. A fate for organic acids, formaldehyde and methanol in cloud water: their biotransformation by microorganisms. Atmospheric Chemistry and Physics 7, 4159-4169.

Barber, P. W., Hill, S. C., 1990. Light Scattering by Particles: Computational Methods. World Scientific, Singapore.

Benincasa, D. S., Barber, P. W., Zhang, J., Hsieh, W., Chang, R. K., 1987. Spatial distribution of the internal and near-field intensities of large cylindrical and spherical scatters. Applied Optics 26, 1348-1356.

Benkelberg, H.-J., Warneck, P., 1995. Photodecomposition of iron(III) hydroxo and sulfato complexes in aqueous solution: Wavelength dependence of OH and SO_4^- quantum yields. Journal of Physical Chemistry 99, 5214-5221.

Bohren, C. F., Huffman, D. R., 1983. Absorption and Scattering of Light by Small Particles. Wiley, New York.

Bouillon, R. C., Miller, W. L., 2005. Photodegradation of dimethyl sulfide (DMS) in natural waters: laboratory assessment of the nitrate-photolysis-induced DMS oxidation. Environmental Science & Technology 39, 9471-9477.

Buxton, G. V., Greenstock, C. L., Helman, W. P., Ross, A. B., 1988. Critical review of rate constants for reactions of hydrated electrons, hydrogen atoms and hydroxyl radicals ($^{\bullet}OH/^{\bullet}O^-$) in aqueous solution. Journal of Physical and Chemical Reference Data 17, 1027-1284.

Chiron, S., Barbati, S., Khanra, S., Dutta, B. K., Minella, M., Minero, C., Maurino, V., Pelizzetti, E., Vione, D., 2009. Bicarbonate-enhanced transformation of phenol upon irradiation of hematite, nitrate, and nitrite. Photochemical & Photobiological Sciences 8, 91-100.

Chylek, P., Pendleton, J. D., Pinnick, R. G., 1985. Internal and near-surface scattered field of a spherical particle at resonant conditions. Applied Optics 24, 3940-3942.

Dang, L. X., Chang, T.-M., Roeselová, M., Garrett, B. C., Tobias, D. J., 2006. On NO_3^--H_2O interactions in aqueous solutions and at interfaces. Journal of Chemical Physics 124, 066101-1 – 066101-3.

Das, R., Dutta, B. K., Maurino, V., Vione, D., Minero, C., 2009. Suppression of inhibition of substrate photodegradation by scavengers of hydroxyl radicals: the solvent-cage effect of bromide on nitrate photolysis. Environmental Chemistry Letters 7, 337-342.

Finlayson-Pitts, B. J., Pitts, J. N., Jr., 2000. Chemistry of the Upper and Lower Atmosphere - Theory, Experiments, and Applications, Academic Press, San Diego..

Frank, R., Klöpffer, W., 1988. Spectral solar photon irradiance in Central Europe and the adjacent North Sea. Chemosphere 17, 985-994.

Furlan, A., 1999. Photodissociation of surface-active species at a liquid surface: a study by time-of-flight spectroscopy. Journal of Physical Chemistry B 103, 1550-1557.

Goldstein, S., Rabani, J., 2007. Mechanism of nitrite formation by nitrate photolysis in aqueous solutions: The role of peroxynitrite, nitrogen dioxide, and hydroxyl radical. Journal of the American Chemical Society 129, 10597-10601.

Hale, G. M., Querry, M. R., 1973. Optical constants of water in the 200-nm to 200-micrometer wavelength region. Applied Optics 12, 555-563.

Hanson, D. R., Burkholder, J. B., Howard, C. J., Ravishankara, A. R, 1992. Measurement of hydroxyl and hydroperoxy radical uptake coefficients on water and sulfuric acid surfaces. Journal of Physical Chemistry 96, 4979–4985.

Harrison, M. A. J., Healk, M. R., Cape, J. N., 2005. Evaluation of the pathways of tropospheric nitrophenol formation from benzene and phenol using a multiphase model. Atmospheric Chemistry and Physics 5, 1679-1695.

Hu, J., Shi, Q., Davidovits, P., Worsnop, D. R., Zahniser, M. S., Kolb, C. E., 1995. Reactive uptake of Cl_2(g) and Br_2(g) by aqueous surfaces as a function of $Br^-$and I^- ion concentration – The effect of chemical reaction at the interface. Journal of Physical Chemistry 99, 8768-8776.

Jacob, D., 2000. Heterogeneous chemistry and tropospheric ozone. Atmospheric Environment 34, 2131-2159.

Jungwirth, P., Tobias, D. J., 2006. Specific ion effects at the air/water interface. Chemical Reviews 106, 1259-1281.

Khanra, S., Minero, C., Maurino, V., Pelizzetti, E., Dutta, B. K., Vione, D., 2008. Phenol transformation induced by UVA photolysis of the complex $FeCl^{2+}$. Environmental Chemitry Letters 6, 29-34.

Kieber, R. J., Seaton, P. J., 1996. Determination of subnanomolar concentrations of nitrite in natural waters. Analytical Chemistry 67, 3261-3264.

Knipping, E. M., Lakin, M. J., Foster, K. L., Jungwirth, P., Tobias, D. J., Gerber, R. B., Dabdub, D., Finlayson-Pitts, B. J., 2000. Experiments and simulations of ion-enhanced interfacial chemistry on aqueous NaCl aerosols. Science 288, 301-306.

Kuhn, H. J., Braslavsky, S. E., Schmidt, R., 2004. Chemical actinometry. Pure and Applied Chemistry 76, 2105-2146.

Liu, Y., Ivanov, A. V., Molina, M. J., 2009. Temperature dependence of $^{\bullet}$OH diffusion in air and He. Geophysical Research Letters 36, L03816.

Mack, J., Bolton, J. R., 1999. Photochemistry of nitrite and nitrate in aqueous solution: A review. Journal of Photochemistry and Photobiology A: Chemistry 101, 89-103.

Madronich, S., 1987. Photodissociation in the atmosphere. 1. Actinic flux and the effect of ground reflection and clouds. Journal of Geophysical Research 92, 9740-9752.

Marinoni, A., Laj, P., Sellegri, K., Mailhot, G., 2004. Cloud chemistry at the puy de Dôme: variability and relationships with environmental factors. Atmospheric Chemistry and Physics 4, 715-728.

Mark, G., Korth, H.-G., Schuchmann, H.-P., von Sonntag, C., 1996. The photochemistry of aqueous nitrate ion revisited. Journal of Photochemistry and Photobiology A: Chemistry, 101, 89-103.

Martell, A. E., Smith, R. M. Motekaitis, R. J., 1997. Critically selected stability constants of metal complexes database, version 4.0.

Mazellier, P., Mailhot, G., Bolte, M., 1997. Photo-chemical behaviour of the iron(III)/2,6-dimethylphenol system. New Journal of Chemistry 21, 389-397.

Mayer, B., Madronich, S., 2004. Actinic flux and photolysis in water droplets: Mie calculations and geometrical optics limit. Atmospheric Chemistry Physics 4, 2241-2250.

Minero, C., Maurino, V., Bono, F., Pelizzetti, E., Marinoni, A., Mailhot, G., Carlotti, M. E., Vione, D., 2007. Effect of selected organic and inorganic snow and cloud components on the photo-chemical generation of nitrite by nitrate irradiation. Chemosphere 68, 2111-2117.

Minofar, B., Jungwirth, P., Das, M. R., Kunz, W., Mahiuddin, S. J., 2007. Propensity of formate, acetate, benzoate, and phenolate for the aqueous solution/vapor interface: Surface tension measurements and molecular dynamics simulations. Journal of Physical Chemistry C. 111, 8242-8247.

Nissenson, P., Knox, C. J. H., Finlayson-Pitts, B. J., Phillips, L. F., Dabdub, D., 2006. Enhanced photolysis in aerosols: evidence for important surface effects. Physical Chemistry Chemical Physics 8, 4700-4710.

Quan, X., Fry, E. S., 1995. Empirical equation for the index of refraction of seawater. Applied Optics 34, 3477-3480.

Ray, A. K., Bhanti, D. D., 1997. Effect of optical resonances on photo-chemical reactions in microdroplets. Applied Optics 36, 2663-2674.

Ruggaber, A., Dlugi, R., Bott, A., Forkel, R., Herrmann, H., Jacobi, H.-W., 1997. Modelling of radiation quantities and photolysis frequencies in the aqueous phase in the troposphere. Atmospheric Environment 31, 3137-3150.

Sadiki, M., Quentel, F., Elléouet, C., Huruguen, J.-P., Jestin, J., Andrieux, D., Olier, R., Privat, M., 2003. Coadsorption at the air/water interface likely explains some pollutants transfer to the atmosphere: benzene and lead case. Atmospheric Environment 37, 3551–3559.

Salvador, P., Curtis, J. E., Tobias, D. J., Jungwirth, P., 2003. Polarizability of the nitrate anion and its solvation at the air/water interface. Physical Chemistry Chemical Physics 5, 3752-3757.

Schwartz, S. E., 1986. Mass-transport considerations pertinent to aqueous phase reactions of gases in liquid-water clouds, in: Jaeschke, W. (Ed.), Chemistry of Multiphase Atmospheric Systems, NATO ASI Series, G6, pp. 415-471.

Thomas, J. L., Roeselová, M., Dang, L. X., Tobias, D. J., 2007. Molecular dynamics simulations of the solution-air interface of aqueous sodium nitrate. Journal of Atmospheric Chemistry 111, 3091–3098.

Vacha, R., Slavicek, P., Mucha, M., Finlayson-Pitts, B. J., Jungwirth, P., 2004. Adsorption of atmospherically relevant gases at the air/water interface: Free energy profiles of aqueous solvation of N_2, O_2, O_3, OH, H_2O, HO_2, and H_2O_2. Journal of Physical Chemistry A 108, 11573-11579.

Vacha, R., Jungwirth, P., Chenb, J., Valsaraj, K., 2006. Adsorption of polycyclic aromatic hydrocarbons at the air-water interface: Molecular dynamics simulations and experimental atmospheric observations. Physical Chemistry Chemical Physics 8, 4461-4467.

Vione, D., Maurino, V., Minero, C., Pelizzetti, E., Harrison, M.A.J., Olariu, R.I., Arsene, C., 2006. Photo-chemical reactions in the tropospheric aqueous phase and on particulate matter. Chemical Society Reviews 35, 441-453.

Vione, D., Minero, C., Hamraoui, A., Privat, M., 2007. Modelling photo-chemical reactions in atmospheric water droplets: An assessment of the importance of surface processes. Atmospheric Environment 41, 3303-3314.

Vione, D., Maurino, V., Minero, C., Duncianu, M., Olariu, R. I., Arsene, C., Sarakha, M., Mailhot, G., 2009a. Assessing the transformation kinetics of 2- and 4-nitrophenol in the atmospheric aqueous phase. Implications for the distribution of both nitroisomers in the atmosphere. Atmospheric Environment 43, 2321-2327.

Vione, D., Khanra, S., Cucu Man, S., Maddigapu, P.R., Das, R., Arsene, C., Olariu, R.I., Maurino, V., Minero, C., 2009b. Inhibition vs. enhancement of the nitrate-induced phototransformation of organic substrates by the $^{\bullet}OH$ scavengers bicarbonate and carbonate. Water Research 43, 4718-4728.

Warneck, P., 1999. The relative importance of various pathways for the oxidation of sulphur dioxide and nitrogen dioxide in sunlit continental fair weather clouds. Physical Chemistry Chemical Physics 1, 5471-5483.

Warneck, P., Wurzinger, C., 1988. Product quantum yields for the 305-nm photodecomposition of NO_3^- in aqueous solution. Journal of Physical Chemistry 92, 6278-6283.

Wingen, L. M., Moskun, A. C., Johnson S. N., Thomas, J. L., Roeselova, M., Tobias, D. J., Kleinman, M. T., Finlayson-Pitts, B. J., 2008. Enhanced surface photochemistry in chloride-nitrate ion mixtures. Physical Chemistry Chemical Physics 10, 5668-5677.

Winter, M., Benjamin, I., 2004. Photodissociation of ICN at the liquid/vapor interface of water. Journal of Chemical Physics 121, 2253-2263.

Zellner, R., Exner, M., Herrmann, H., 1990. Absolute OH quantum yields in the laser photolysis of nitrate, nitrite and dissolved H_2O_2 at 308 and 351 nm in the temperature range 278-353 K. Journal of Atmospheric Chemistry 10, 411-425.

Zepp, R. G., Hoigné, J., Bader, H., 1987. Nitrate-induced photooxidation of trace organic chemicals in water. Environmental Science & Technology 21, 443-450.

Table 1. Photolysis quantum yields of $FeOH^{2+}$ at different wavelength values. The quantum yields that include the solvent-cage effect, relevant to the solution bulk, are based on the data of Benkelberg and Warneck (1995). The quantum yields without the solvent-cage effect, relevant to the air-water interface, are based on the experimental results of this work and the additional hypothesis that the wavelength trend is similar to that of the bulk process (with the solvent-cage effect).

λ, nm	$\Phi(FeOH^{2+})$, solvent-cage	$\Phi(FeOH^{2+})$, no solvent-cage
290	0.21	1.0
300	0.16	1.0
310	0.14	1.0
320	0.12	0.85
330	0.11	0.74
340	0.10	0.63
350	0.07	0.45
360	0.04	0.18
370	0.04	0.18

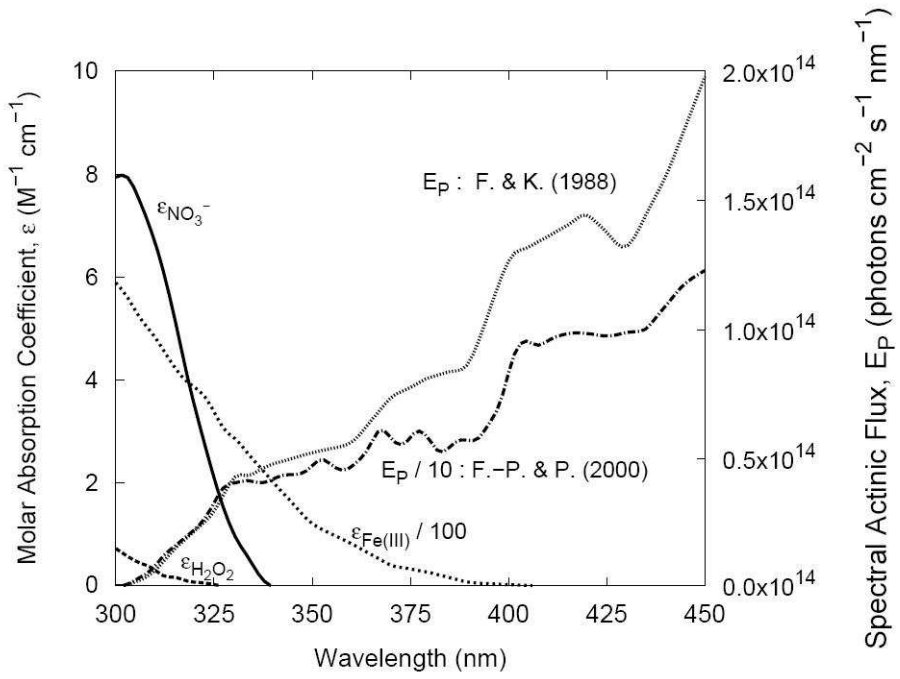

Figure 1. Absorption spectra of nitrate, H_2O_2 and Fe(III), the latter at pH 2.5. Sunlight spectra according to Finlayson-Pitts and Pitts (2000) (F.-P. & P.) and Frank and Klöpffer (1988) (F. & K.).

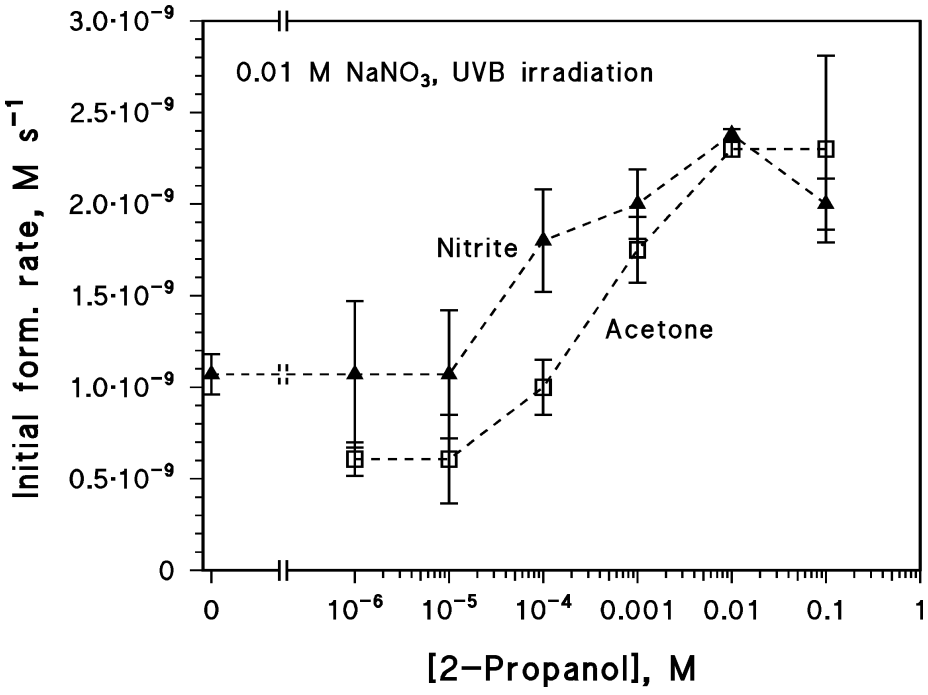

Figure 2. Initial formation rates of nitrite and acetone as a function of the concentration of 2-propanol, upon UVB irradiation of 0.01 M $NaNO_3$. Note the logarithmic scale and the break in the *x*-axis.

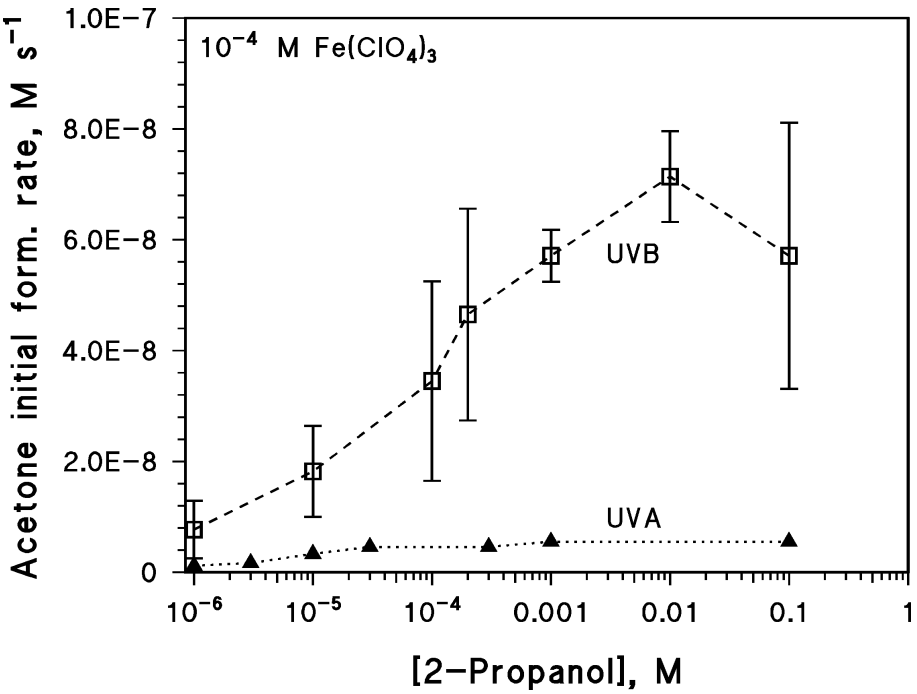

Figure 3. Initial formation rates of acetone as a function of the concentration of 2-propanol, upon irradiation (UVB or UVA) of 0.1 mM $Fe(ClO_4)_3$. Note the logarithmic scale in the *x*-axis.

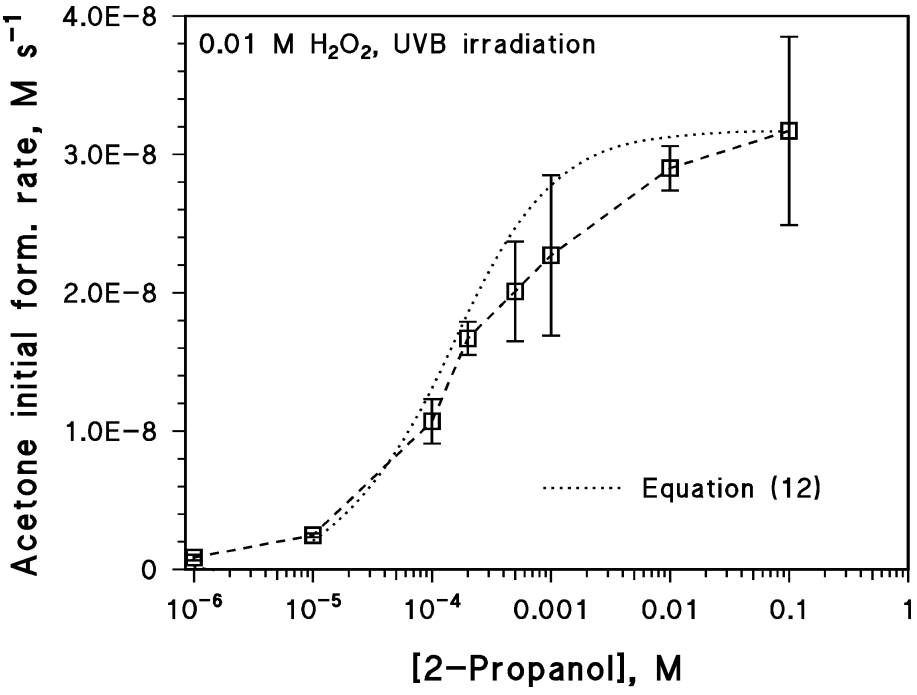

Figure 4. Initial formation rates of acetone as a function of the concentration of 2-propanol, upon UVB irradiation of 0.01 M H_2O_2. Note the logarithmic scale in the *x*-axis.

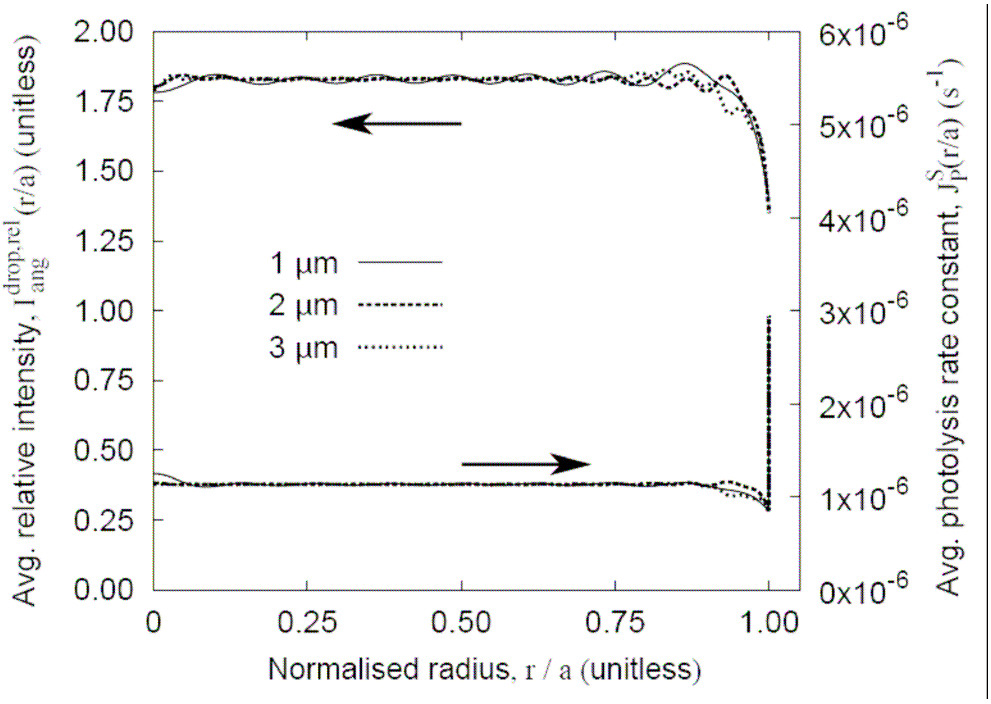

Figure 5. The angle- and wavelength-averaged relative intensity ($I_{ang}^{drop,rel}$) and angle-averaged photolysis rate constant for nitrate ($J_P^{NO_3^-}$) as a function of normalized distance *r*/*a* from the droplet center. The water droplets of radius 1 µm, 2µm, and 3µm contain 10^{-4} M nitrate. The spectrum from Finlayson-Pitts and Pitts (2000) is used to calculate $I_{ang}^{drop,rel}$.

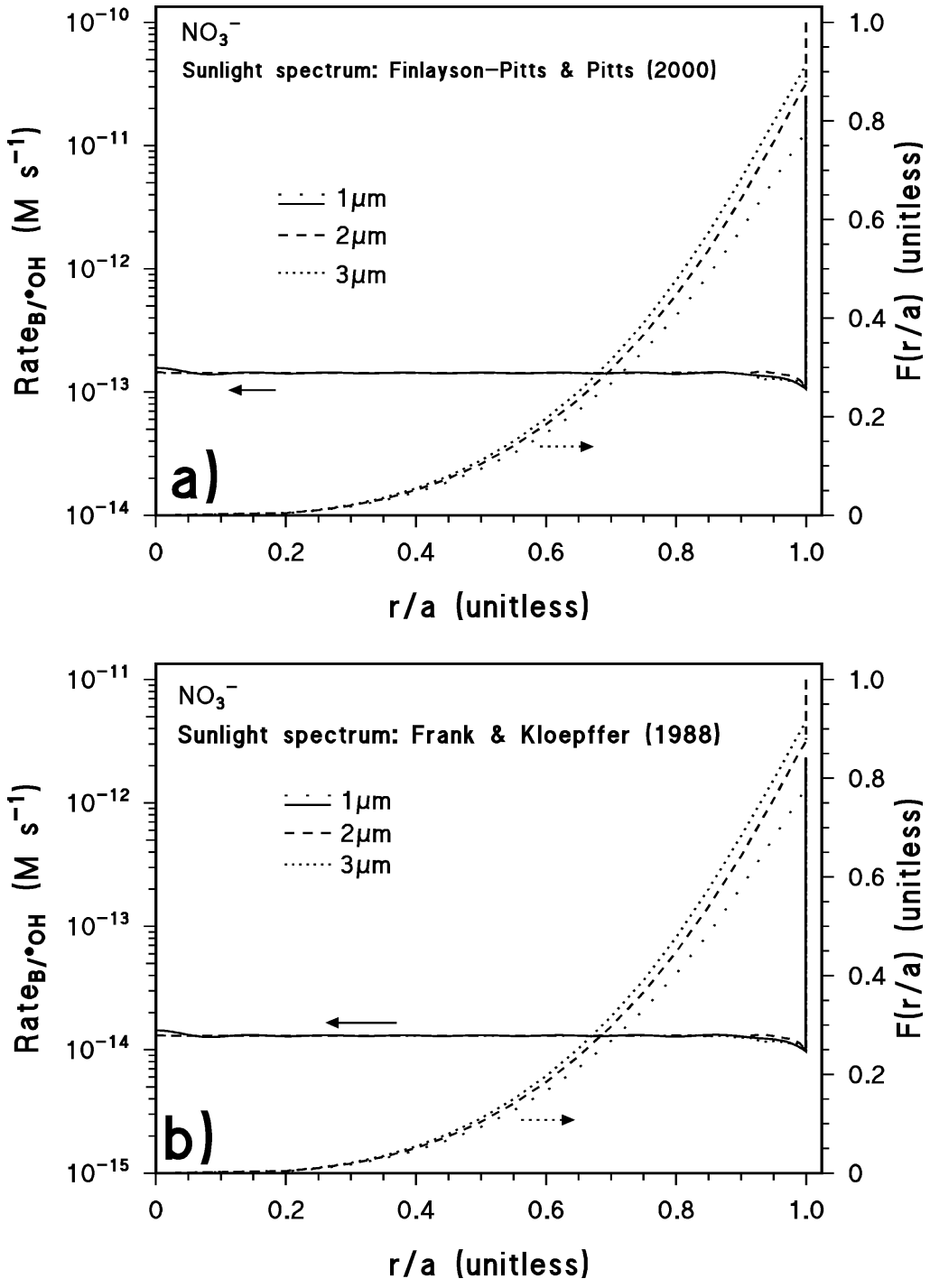

Figure 6. Trends in the aqueous reaction rate between benzene and $^{\bullet}$OH, $Rate_{B/\bullet OH}$, (eq. 13) and in $F(r/a)$ (eq. 14) for 0.1 mM nitrate, as a function of the normalized distance r/a from the droplet center. The figure reports data for spherical droplets of radius a = 1, 2 and 3 μm. Figure (a) uses the sunlight spectrum as reported by Finlayson-Pitts and Pitts (2000) while Figure (b) uses the sunlight spectrum as reported by Frank and Klöpffer (1988).

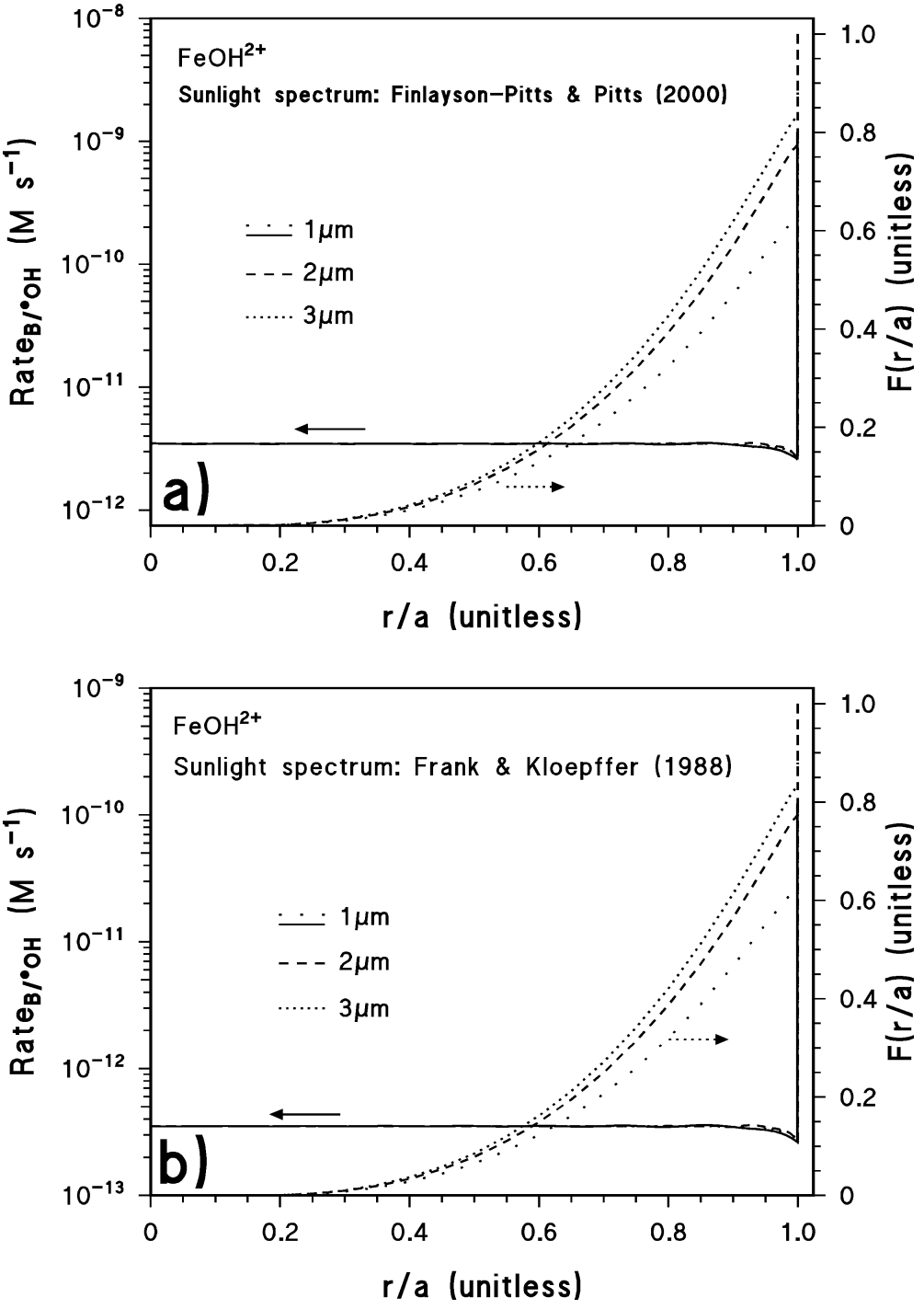

Figure 7. Trends in the aqueous reaction rate between benzene and •OH, $Rate_{B/\bullet OH}$, (eq. 13) and in $F(r/a)$ (eq. 14) for 1 μM $FeOH^{2+}$, as a function of the normalized distance r/a from the droplet center. The figure reports data for spherical droplets of radius a = 1, 2 and 3 μm. Figure (a) uses the sunlight spectrum as reported by Finlayson-Pitts and Pitts (2000) while Figure (b) uses the sunlight spectrum as reported by Frank and Klöpffer (1988).

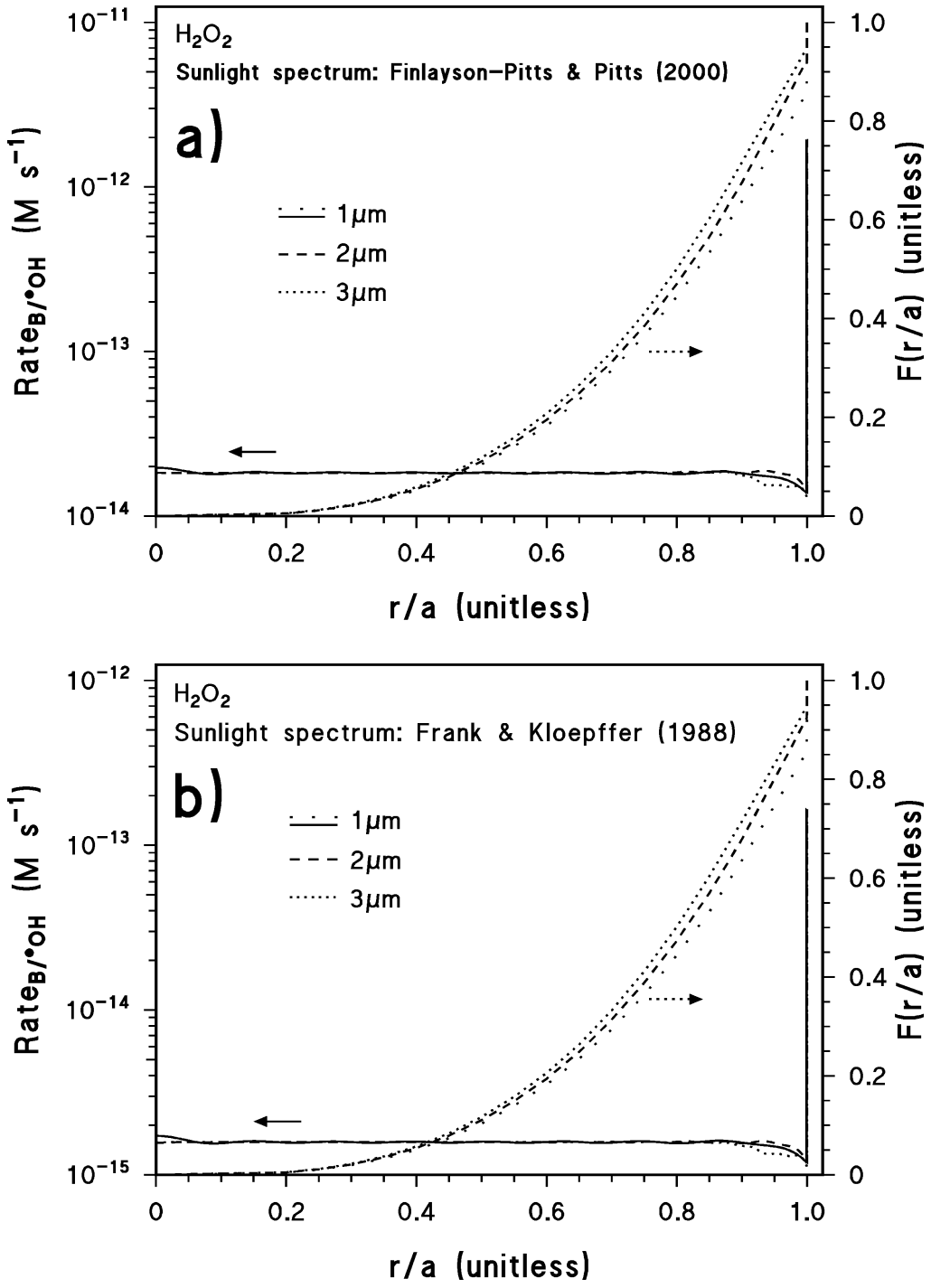

Figure 8. Trends in the aqueous reaction rate between benzene and $^{\bullet}OH$, $Rate_{B/\bullet OH}$, (eq. 13) and in $F(r/a)$ (eq. 14) for 10 μM H_2O_2, as a function of the normalized distance r/a from the droplet center. The figure reports data for spherical droplets of radius a = 1, 2 and 3 μm. Figure (a) uses the sunlight spectrum as reported by Finlayson-Pitts and Pitts (2000) while Figure (b) uses the sunlight spectrum as reported by Frank and Klöpffer (1988).